

Received January 10, 2020, accepted January 22, 2020, date of publication January 28, 2020, date of current version February 10, 2020.

Digital Object Identifier 10.1109/ACCESS.2020.2969969

A Passive RFID Temperature Sensing Antenna With Liquid Crystal Elastomer Switching

YOUSUF SHAFIQ¹, (Student Member, IEEE), JULIA HENRICKS², CEDRIC P. AMBULO², TAYLOR H. WARE¹⁰², AND STAVROS V. GEORGAKOPOULOS¹⁰¹, (Senior Member, IEEE)
1 Department of Electrical and Computer Engineering, Florida International University, Miami, FL 33174, USA

Corresponding author: Stavros V. Georgakopoulos (georgako@fiu.edu)

This research was supported by the National Science Foundation under grants ECCS 1711467 and 1711383.

ABSTRACT An autonomous and continuously operating Radio Frequency Identification (RFID) temperature sensor is designed, manufactured, and tested. This sensor is battery-free and can detect temperature threshold crossings for multiple (room-to-cold and cold-to-room) temperature cycles, respectively. The proposed sensor conveys temperature threshold crossings through the controlled switching of its operating frequency within the 902-928 MHz Ultra High Frequency (UHF) RFID band. For the first time, shape morphing cold-temperature reactive Liquid Crystal Elastomers (LCEs), which provide reversible actuation, are utilized. The proposed sensor design consists of a patch antenna with a customized slot. A passive mechanical switch is connected across this slot and provides the frequency switching as it is activated and deactivated. The integration of this switch with the antenna is achieved using a co-simulation method. Furthermore, the cold-temperature reactive LCE triggers the switch when a temperature violation has occurred, thereby switching the operating frequency of the sensor based on temperature changes. Additionally, a high-dielectric constant substrate and a single matching network that operates at two discrete frequencies are used to design our compact frequency-domain temperature sensor. Moreover, based on the RFID platform, this sensor operates effectively in close-proximity to other sensors. Also, is provides identification and temperature information through an autonomous, continuous, and cost-effective design. Therefore, the proposed sensor has the potential for operation in the Internet of Things (IoTs) applications, where large amounts of data is collected from numerous sensors to extract valuable information for the benefit of users, manufacturers, and delivery companies in the virtual domain of the internet. Finally, ANSYS HFSS and Circuit Designer are used for the simulation modeling. The performance of our sensor is validated using measurements and simulations that agree very well.

INDEX TERMS RFID temperature sensor, liquid crystal elastomers (LCEs), RFID impedance matching, dual-frequency complex matching network design, frequency reconfigurable patch antenna, Internet of Things (IoTs).

I. INTRODUCTION

The Cold-Supply-Chain (CSC) deals with the delivery of perishable foods and pharmaceutical products that must be kept in an uninterrupted and controlled temperature environment from the manufacturer to the end-user [1]. Additionally, the CSC ensures the longevity, safety, and quality of such items. The temperatures at which these items are maintained at during the delivery cycle range from -1° to 10° C [2], [3]. Conversely, when foods, such as, fruits,

The associate editor coordinating the review of this manuscript and approving it for publication was Kai Yang

vegetables, and meats, are exposed to excessively high or low temperatures, they experience discoloration and loss of nutrients [2]. Also, if medications are not kept in the appropriate temperature range, they lose their potency [3]. Currently, the CSC is continuously developing due to growing populations, developing nations, technology advancements, and federal regulations promoting the use of the CSC [4]. As a result, 65% of the retail food market presently consists of fresh-food products [5].

Presently, temperature monitoring is conducted at three points during the delivery cycle from the supplier to the consumer [6]; namely, at the sending and receiving stations, and

²Department of Bioengineering, University of Texas at Dallas, Richardson, TX 75080, USA



at the transportation containers. Temperature conditions at each of these discrete locations are recorded and then used to assess the overall condition of the perishable goods. However, a significant problem within this process of monitoring exists. That is, the temperature conditions due to any anomalies at any intermediate stage are unaccounted. Common anomalies that often occur in the CSC are malfunctioning refrigeration equipment, extended wait-times at cargo bays, and operator errors (e.g., constantly opening and/or leaving the container doors open, failure to pre-cool, and road accidents) [7]. Additionally, the improper placement of perishable items within the delivery vehicle and inadequate packaging also inhibit perishable products from being maintained at the proper temperature during the delivery cycle [2], [7]. Hence, at some point along the delivery cycle a perishable item could be exposed to unacceptable temperature conditions without the knowledge of the end-user. As a result of these common anomalies, 30% of fresh-food products are damaged during transit [6]. In 2015, the global sales of organic foods amounted to approximately \$81.6 billion [8]. Therefore, due to the safety and financial risks associated with the delivery of perishable foods and pharmaceuticals in the CSC, an effective sensor solution to monitor such essential foods and medications is necessary.

Radio Frequency Identification (RFID) technology provides a favorable platform with an established and standardized communication protocol that can support passive wireless sensing in real-time for continuous monitoring [9, pp. 43-46]. The prevalent use of RFID technology is in cataloging, identifying, and tracking people and/or objects [9, pp. 15-22]. However, this technology can also have a dominant impact in the application of sensing as well [10]. Sensing using RFID technology can be acquired in two ways. The first method involves incorporating a separate sensing IC which performs the detection. This is then translated to the digital domain and transferred to the reader wirelessly. The data is then decoded, using an additional layer of software to convey the tracked information. Unfortunately, this design methodology accounts for active and semi-active tag designs, which require power sources on the tags (i.e., batteries). The second method consists of designing the RFID antenna so that it serves as both the sensing and communication element. This design methodology is promising as it provides purely passive (i.e., battery-free) and inexpensive RFID tags. Therefore, the latter method is pursued here to produce a passive RFID temperature sensor for the CSC.

Furthermore, RFID technology can effectively operate in dense environments (i.e., hundreds of RFID tags in close-proximity); therefore, it is suitable for collecting data on a large scale to provide useful information [11]. Specifically, RFID readers can collect and relay data through the internet so that people and objects can be identified, tracked, and monitored globally, automatically, and in real-time. This system of extracting useful data from thousands of sensors scattered throughout the world is the Internet of Things (IoTs) [12], [13]. Examples of applications that utilize the IoTs

include the investigation of the behavior pattern of people moving throughout a structure [13], object location tracking [14]–[16], improved automated traffic control at intersections [17], enhanced personal based healthcare [18], and efficient supply chain operations [11]. For example, in the supply chain, each product can have an RFID tag with a unique identifier code for tracking. In this case, each phase of the supply chain would need to be equipped with a reader. Through this dynamic processing, suppliers and consumers would be able to examine the products circulation history. Moreover, manufacturers could share and compare the status of the products' circulation with manufacturing plants in real-time to improve efficiency [19].

Passive RFID tags for temperature monitoring have been examined before. For example, a passive RFID tag for heat sensing applications was developed by researchers in [20]. This sensor consists of a customized designed antenna that is placed on a substrate of paraffin wax. As the paraffin wax begins to melt due to high temperature exposure, the properties are altered, which de-tunes the operating frequency of the tag in order to detect changes in temperature. Additionally, a sensor was developed in [6] based on shape memory polymers to detect changes in temperature through frequency shifts. Another temperature sensor was presented in [21], which consists of an antenna that can switch between turning on one or two RFID ICs (depending on the temperature) using a shape memory alloy switch. All these designs are costeffective and can be suitable for CSC applications. However, their capabilities are limited, since they can be used only once, or they must be reset after each time they are triggered by a temperature variation. Hence, these are not convenient solutions. Pragmatic designs should be reusable and be able to detect multiple temperature violations over time without any maintenance or resetting.

Moreover, commercially available semi-active and active RFID tags have been developed for temperature monitoring in the CSC [22]. For example, the Sensor Temperature Dog bone from Smarttrac [23]. This tag consists of an RFID IC, which also serves as the temperature sensor. The temperature information is digitized and wirelessly communicated to the reader. Another example is the Freshtime Sensor RFID Classic Tag, which is a semi-passive RFID tag from Infratab [24]. This sensor utilizes a separate onboard temperature IC sensor, which takes temperature samples and integrates them over time to predict the shelf-life of a product. Finally, IDS Microchip AG has developed the IDS-SL13A, which is a single-chip temperature sensor and data logger [25]. Even though these sensors can monitor fresh-product goods in the CSC, each of them have limitations. In summary, they require additional specialized software, are expensive, require batteries, or do not provide real-time readings. These drawbacks cause vulnerabilities in the robustness of the CSC process.

Therefore, a new CSC wireless sensor is needed that is able to: (a) monitor temperature of individual items or crates, (b) operate without batteries (i.e., passive) in order to provide long operational life and cost-effectiveness,



(c) provide continuous temperature monitoring even for reversible fluctuations (e.g., able to detect multiple cycles of room-to-cold and cold-to-room variations), (d) operate autonomously and without requiring any form of resetting, and (e) fit in a small package (i.e., compact) so that it can be conveniently attached to various CSC items. In this work, a compact and passive RFID temperature sensor with these needed features is developed, fabricated, and measured.

Our design utilizes a patch antenna with a slot that is integrated with a switch. The switch is controlled by state-of-the art cold-temperature-responsive Liquid Crystal Elastomers (LCEs). The state of the switch (activated or not) determines the operating frequency of our RFID sensor. Therefore, the proposed sensor can detect changes in temperature through shifts in its operational frequency. Also, LCEs are temperature responsive polymers that are programmable and reversible, [26], which enables our proposed sensor to monitor temperature continuously (i.e., it is not a single-use sensor) and autonomously (i.e., it does not need resetting), while being passive (i.e., battery-free). Therefore, our sensor is suitable for IoT applications due to its functionality, compact form-factor, and ability to operate in crowded environments (i.e., numerous other RFID sensors can be present nearby).

In summary, our work develops for the first time an autonomous and continuously operating RFID temperature sensor that is battery-free using new shape morphing cold-temperature reactive Liquid Crystal Elastomers (LCEs), which provide reversible actuation. Our sensor uses a patch antenna with a slot and it can detect temperature threshold crossings for multiple (room-to-cold and cold-to-room) temperature cycles through the controlled switching of its operating frequency within UHF RFID band.

Section II of this paper highlights the design considerations along with adapting RFID technology for temperature sensing. Section III discusses the theory and design of our Liquid Crystal Elastomers (LCEs). Subsequently, Section IV presents the design of our patch antenna. Section V provides the details on the fixture that houses and translates the force of the LCE array. Furthermore, Section VI discusses the matching network that is needed to enable operation at two discrete frequencies. Finally, Section VII examines the operation of our sensor in actual environmental conditions.

II. DESIGN CONSIDERATIONS AND OPERATIONAL OVERVIEW

A. SENSING METHODOLOGY WITH RFID TECHNOLOGY

Our sensor is designed to reversibly operate at different frequencies depending on the temperature. Specifically, our sensor operates in the high-end of the RFID band at room temperature (state 1) and in the lower-end of the RFID band at cold temperatures (state 2; approximately -9° C).

B. IMPEDANCE MATCHING AND THE POWER TRANSMISSION COEFFICIENT (PTC)

In the design of the proposed sensor the Alien Higgs III SOT RFID IC was used [27]. According to [6] and [28],

the nominal input impedance is taken as $Z_{IC}=18-164j$ across the UHF RFID band. Moreover, a vast number of commercially available RFID ICs have similar complex input impedances [29, pp. 51-54]. For proper operation, it is essential to design an impedance matching network between the antenna and the RFID IC [29, p. 50] [30, p. 78]. The impedances of the RFID antenna (Z_A) and RFID IC (Z_{IC}) are defined respectively as follows:

$$Z_A = R_A + i X_A \tag{1}$$

$$Z_{IC} = R_{IC} + jX_{IC} \tag{2}$$

The power wave reflection coefficient between the antenna and the IC is defined as [31]–[33]:

$$\Gamma = \frac{Z_{A} - Z_{IC}^{*}}{Z_{A} + Z_{IC}} \tag{3}$$

Furthermore, the Power Transmission Coefficient (PTC) is specified as [32], [34, pp. 69-71]:

$$\tau = 1 - |\Gamma|^2 \tag{4}$$

Finally, incorporating (1) and (2) into (3) and substituting the result into (4) the following form of the PTC is derived:

$$\tau = \frac{4R_A R_{IC}}{|Z_A + Z_{IC}|^2} \tag{5}$$

This relation is a figure of merit that is used here. It signifies the degree of matching between the antenna and the RFID IC, where $0 \le \tau \le 1$. In the case when $\tau = 1$, a conjugate match $(Z_A = Z_{IC}^*)$ is obtained that provides maximum power transfer to the IC [6], [30, p. 78].

C. SENSOR ARCHITECTURE

In this section, we provide a functional overview of the proposed sensor design. A patch antenna with a slot is designed so that a switch can be placed across the slot to provide the desired frequency switching. Notably, in RF design, MEMS or PIN diodes have been used as switches [35], [36]. However, these are active devices (i.e., they require power sources). To provide a purely passive design, our sensor uses an ultra-subminiature mechanical switch (USMS), [37], that shorts or opens the antenna's slot. It should be noted that when the switch is ON (i.e., pressed or activated) it provides an approximate open across the slot and when the switch is OFF (i.e., de-pressed or deactivated) it provides an approximate short across the slot. Since the switch provides an approximate short and open at its OFF and ON positions, respectively, incorporation of this switch in our antenna design requires full RF characterization of the performance of the switch, which is done in Section IV.A. In addition, reversible LCEs that react to cold-temperatures (approximately -9° C) are developed for the first time to control this switch based on temperature. Specifically, an LCE array is designed, where each element consists of a circular cell that is printed in a

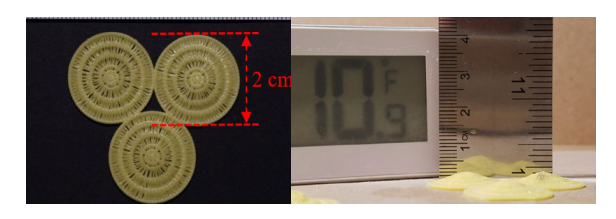


FIGURE 1. Each cell in the LCE array reacts to cold temperature by forming a cone.

radial pattern, as shown in Fig. 1. When exposed to cold-temperatures, each cell in the LCE array forms a cone structure. Together, the array provides the needed force to activate our mechanical switch. A housing is also designed to support and translate the vertical actuating motion of the LCE array to reversibly activate the switch, which is further discussed in Section V. Finally, a matching circuit is designed between our antenna and the RFID IC to support functionality at two discrete frequencies within the RFID band.

III. LIQUID CRYSTAL ELASTOMERS

A. LIQUID CRYSTAL ELASTOMER CHARACTERISTICS

Liquid crystal elastomers are soft materials that undergo a reversible change in shape in response to a change in temperature. This shape change results from the coupling of the order of liquid crystals with the elastic behavior of the polymer network [38]. For these materials to undergo shape change in the absence of a load, the liquid crystal phase of the material, typically the nematic phase, must be aligned during processing. This alignment can be achieved with mechanical stretching, directed self-assembly, or 3D printing [39]–[43]. After processing and crosslinking the material, shape change is most commonly induced by heating the LCE. The shape change on heating of a LCE is a length reduction along the alignment direction and, as the shape change is largely volume conserving, a smaller expansion along the two directions perpendicular to the alignment direction. When the alignment is patterned in a spatially complex manner in a flat film the material often deforms into the third dimension.

B. DESIGNING COLD RESPONSIVE LIQUID CRYSTAL ELASTOMERS

While the shape change of LCEs is typically activated by heating, cooling below the processing temperature induces a shape change that is opposite in sign to the shape change observed on heating. For the design of the cold responsive liquid crystal elastomers, we sought to create a liquid crystal elastomer structure capable of providing the necessary force and displacement to trigger a commercial switch. In prior work, cold response has been demonstrated by LCEs that undergo twisting, but this bending-dominated shape change is intrinsically incapable of producing large forces [44]. It has been shown in prior work that flat films that morph into cones are capable of both large displacement and large work capacity [45]. To create films that form cones on cooling, the material must have excess length form along the radial

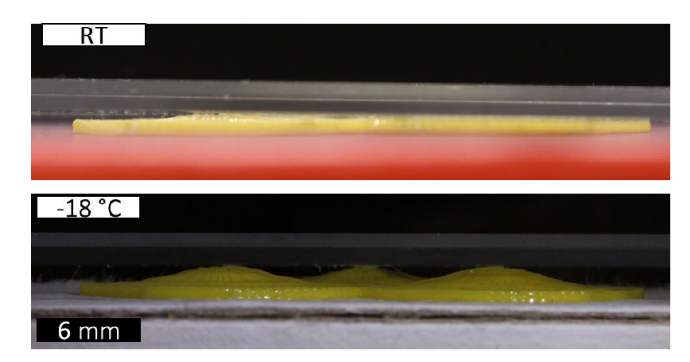


FIGURE 2. The actuation of printed LCEs disks on cooling from room temperature to -18° C. The disks are lifting glass slides with a combined weight of 0.14 N.

direction with respect to the azimuthal direction. This can be achieved by orienting the LCE in a radial pattern [46]. While several methods exist to create LCEs with complex alignment, here we use direct ink write printing. Importantly, direct ink write printing enables the processing of LCE structures with large thickness (>100 μ m), which in turn leads to increased force output. Specifically, we printed three connected LCE disks, with the center of each disk on the vertices of an equilateral triangle with side length (2 cm). Each disk consists of a radial print path 3 layers thick (total thickness approximately 750 μ m). The chemistry of the material and printing parameters were previously described in [41]. This three-disk structure actuates to 3 cones on cooling. These three cones can lift a weight of 0.14 N a distance of 1.5 mm (Fig. 2). This load and displacement is sufficient to actuate the selected switch.

IV. PATCH ANTENNA DESIGN WITH FREQUENCY SWITCHING CONCEPT

The UHF RFID band in the United States is 902 MHz to 928 MHz. This narrow bandwidth of 26 MHz presents a design challenge. Since the goal is to convey temperature threshold crossings through shifts in the frequency of operation, a narrowband antenna is needed. Therefore, a patch antenna is used in our sensor [47]. This antenna is probefed, and it is miniaturized by using a substrate made from a ceramic polymer composite (Rogers TMM 13i) with a high dielectric constant (i.e., $\varepsilon_r = 12.85$) [48]. Such high dielectric constant substrate further compresses the operational bandwidth thereby improving the frequency selectivity of the sensor [49]. Also, to be able to switch the operational frequency of our RFID tag, our patch antenna uses a slot. A short can be added and removed as desired across the slot to obtain on-demand switching of the operational frequency [35].

The addition of a slot on a patch antenna increases its electrical length (L) because the surface currents on the patch must travel a longer path, [35]. In turn, this decreases the resonant frequency of the patch, which is given by [50, p. 266]:

$$f = \frac{c}{2L\sqrt{\varepsilon_{\text{eff}}}} \tag{6}$$



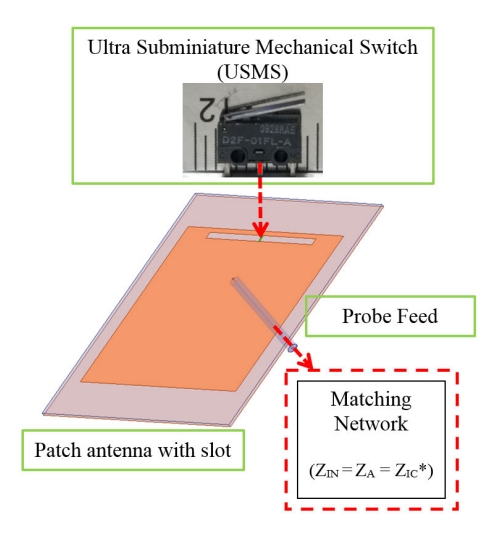


FIGURE 3. The switch is connected across the slot and provides the passive frequency switching capability of the antenna when activated and deactivated.

Furthermore, if a short is placed across the slot, the modified effective electrical length of the patch is once again reduced as the short provides an additional path for the current to flow. This causes the resonant frequency to increase.

It is important to note that the dimension of the slot must be calculated carefully to provide the proper frequency switching within the desired frequency band. The procedure for designing such an antenna is as follows. First, a typical patch antenna is designed at a frequency (930 MHz) that is slightly higher than the desired operating frequency of the antenna when the slot is shorted. Then, using a simulation study with ANSYS HFSS a slot is added to the patch that provides the desired low-frequency operating point within the RFID UHF band (e.g., 902 MHz).

In this research, we apply the above-mentioned concept and our antenna's frequency of operation is switched or controlled by a mechanical switch, which is placed across the patch's slot. Specifically, a passive mechanical single-pole double-throw (SPDT) switch, made by Omron Electronics, is used [37]. Therefore, this switch has three terminals (one input and two outputs) of which only two are utilized to establish either a conduction or isolation mode based on pressing or de-pressing the switch. Due to the SPDT functionality of the switch, the two terminals that are utilized in this design operate in an isolation mode when the switch is pressed (activated or ON) and in conduction mode when the switch is de-pressed (deactivated or OFF). Moreover, this switch does not need biasing as diodes and MEMs, and it is activated by our LCE array that responds to cold temperatures, thereby allowing a battery-free (i.e. passive) frequency-domain RFID temperature sensing tag. A diagram of the sensor setup is shown in Fig. 3.

A. CO-SIMULATION SETUP AND ANTENNA DESIGN

In this section, the characterization and RF modeling of the switch is described, because it cannot be represented as



FIGURE 4. Microstrip test fixture for measuring the switch S-parameters. (Top) fixture without switch for phase compensation. (Bottom) fixture with switch

a perfect short or open circuit at its two operating states. To measure the switch, a microstrip test fixture was designed as shown in Fig. 4. Initially, the test fixture (Fig. 4 top) is measured without the switch to calibrate its electrical length using the open-circuit auto-port extension feature of the E5061B Vector Network Analyzer (VNA). Then, the switch is connected to the fixture and measured on its ON and OFF states with the VNA, as shown in Fig. 4 (bottom). Since the auto-port correction was used, our measurements are now referenced directly to the terminals of the switch and the effects of the test fixture have been de-embedded. The measurements are depicted in Fig. 5, which shows that the switch's insertion loss at its ON and OFF states is approximately 12.5 dB and 2 dB, respectively. As mentioned in Section II.C, the ON (i.e., pressed) and OFF (i.e., de-pressed) states represent approximate open and short states, correspondingly.

To accommodate the switch's model in our simulation, the patch antenna is setup in ANSYS HFSS as a two-port network by placing an additional port across the slot, where

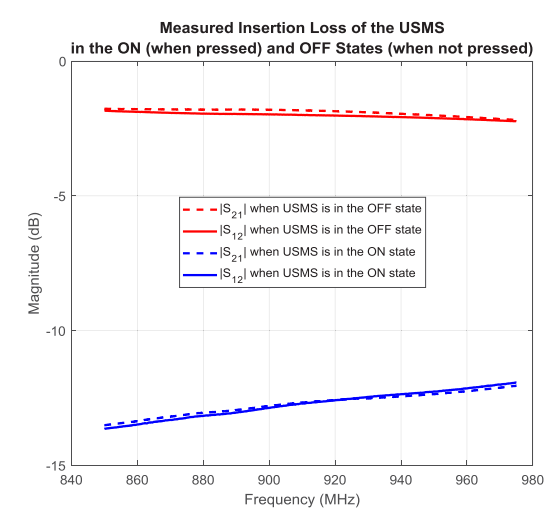


FIGURE 5. Measured insertion loss of the switch at its ON and OFF states.



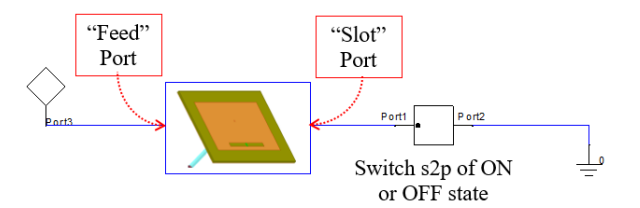


FIGURE 6. ANSYS Circuit Designer setup of the antenna with the switch.

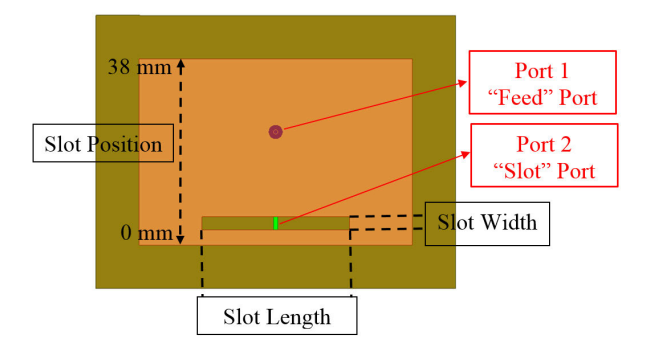


FIGURE 7. A parametric sweep of the slot width, length, and position is conducted using HFSS.

the switch will be placed. Therefore, port 1 will be the "feed" port and port 2 will be the added "slot" port. After the antenna is simulated in ANSYS HFSS, its equivalent two-port network is exported to ANSYS Circuit Designer that is used to merge the antenna simulation results by HFSS and the measured performance of the switch using a co-simulation method [51]. Also, the s2p file corresponding to the measurements of the switch for each state is imported in ANSYS Circuit Designer and applied to the "slot" port, as shown in Figs. 6 and 7. Then, the response of the antenna at the feed port is examined at both ON and OFF states of the switch. Finally, a parametric sweep of the patch's slot length, width, and position is conducted in HFSS, refer to Fig. 7. The performance of each design is then examined in ANSYS Circuit Designer with the switch model to find the design that can provide the desired frequency change between the two states of the switch. Specifically, the chosen design is based on how large the switching bandwidth is (it should be as large as possible but should not exceed the RFID UHF bandwidth which is 26 MHz) and the location of these two switching frequencies (should ideally be within the RFID band of 902-928 MHz). No design can simultaneously fulfill both criteria. Therefore, we choose the design that meets both criteria in the most optimal way. However, to compensate and allow the antenna to operate as ideally as possible, we design a two-stage matching network. The first stage of the matching network shifts the operating frequencies of the antenna to within the RFID band (i.e., 902-928 MHz). The second stage of the matching network matches the 50Ω response at the two operating frequencies to the conjugate input impedance of the RFID IC.

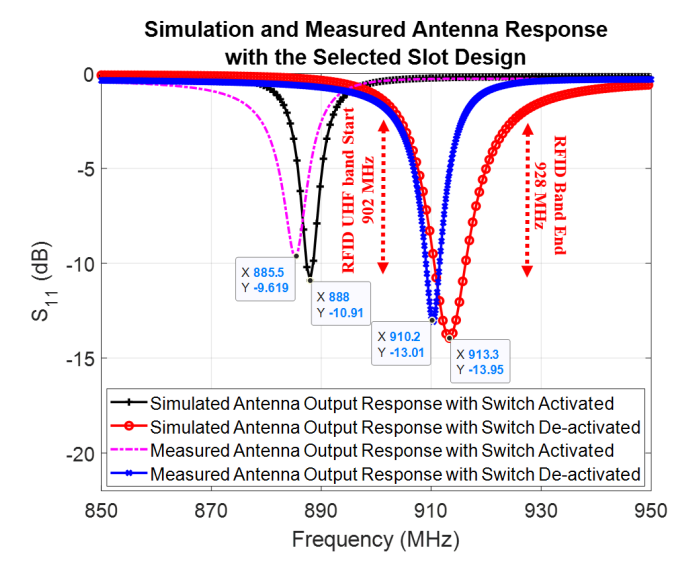


FIGURE 8. Measured and simulated results for the selected antenna design.

The final design has the following dimensions: Slot Length: 34mm, Slot Position: 15mm, and Slot Width: 3mm (see Fig. 7). The frequency response of this design is depicted in Fig. 8, which shows that the operational frequency of our antenna is 913.3 MHz and 888 MHz at the OFF and ON switch states, respectively. There is 25.3 MHz difference between the two frequencies of operation, which allows us to clearly decipher between the two states (i.e., we can reliably determine at which state the antenna works based on its frequency of operation). Notably, the antenna's frequency of operation at the ON state lies outside the RFID UHF band. Therefore, a frequency-shift is required and is achieved using a matching network, which is discussed in the following section. Thus far, it is important to note that we have derived an antenna design which operates at two desired frequencies, which are controlled by the switch.

V. INTEGRATION OF ANTENNA AND LCE ACTUATOR

Our antenna was fabricated on a ceramic polymer composite (Rogers TMM 13i) substrate with a high dielectric constant of 12.85. Subsequently, the switch was soldered across the slot. The prototype is shown in Fig. 9. In this section, we integrate our novel cold-responsive LCE actuator array (shown in Figs. 1 and 2) with the switch connected to our antenna to enable passive temperature sensing. This is accomplished using a 3D printed housing for the LCE array, as shown in Fig. 10. This housing includes two components: (a) an anchored frame that is attached to the base of the switch to provide a static reference for the LCE to apply a force against, and (b) a movable platform that is attached to the dynamic lever of the switch and serves as a platform for the LCE array. According to Section III, the displacement during actuation incurred by cold temperatures (approximately -9° C) on the LCE array is only 1.5 mm. Therefore, our housing for the



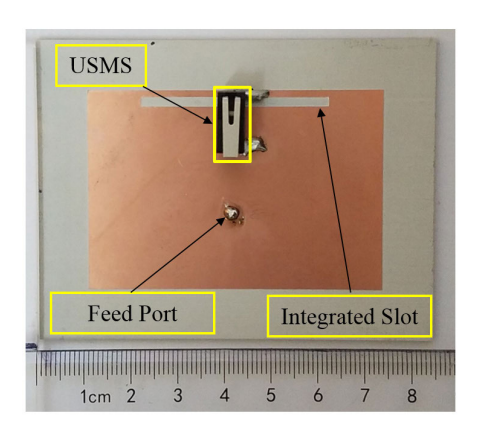


FIGURE 9. Fabricated antenna with the switch soldered across its slot.

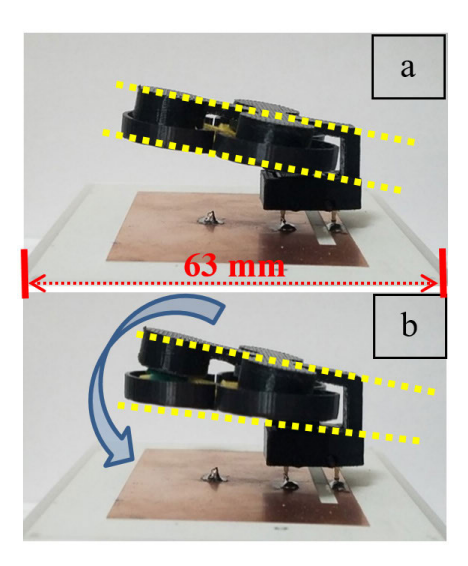


FIGURE 10. 3D printed frame anchored to switch and array platform to support and translate the actuation of the LCE. a) The LCE is at its relaxed state and the switch is at its OFF (de-pressed or deactivated) state. (b) The LCE is actuated, pushing the switch to its ON (pressed or activated) state.

LCE array (shown in Fig. 10) was designed accordingly so that the LCE actuator could reliably control the switch.

The antenna was measured using the Agilent E5071C ENA at the two different states of the switch. The measurements are compared with the simulations in Fig. 8 and they exhibit good agreement thereby validating the accuracy of our co-simulation setup. The slight discrepancy between the measured and simulated results is attributed to the tolerance associated with the Rogers TMM13i substrate used in the design [48]. Also, the measured frequency switching bandwidth of the fabricated design is 24.7 MHz, which agrees well with the simulated one of 25.3 MHz. This bandwidth is slightly less than the RFID UHF bandwidth of 26 MHz, which ensures that the maximum PTC will occur for operating frequencies within the RFID UHF band.

VI. MATCHING NETWORK DESIGN

Thus far, we have designed a passive antenna which switches operating frequencies based on temperature. The design

consists of a switch, which is actuated by novel LCEs and a customized slotted patch antenna. To complete the sensor design, we must address the following two design issues: (a) the antenna currently operates outside the RFID band in one of the switch's states, as shown in Fig. 8, and (b) the antenna impedance has not been matched to the conjugate of the RFID IC input impedance and this needs to be done at both the ON and OFF states of the switch. Here, we discuss a two-stage matching network, where the first and second stages address the design issues of (a) and (b), respectively. This method provides a systematic approach to successfully match the antenna to the RFID IC for both states of the switch.

A. FIRST STAGE MATCHING

It is helpful to first recognize that our antenna (see Fig. 9) behaves as two different antennas on a single platform. Specifically, when the switch is at its OFF state the antenna operates at 910.2 MHz, and when the switch is at its ON state the antenna operates at 885.5 MHz (see Fig. 8).

The goal of the first stage of the matching network is to shift the switching-bandwidth of the design to within the RFID operating band. The technique used here, involves the matching of the input load impedance at the desired operating frequency (e.g., a frequency within the RFID band) to 50 Ω . However, since this design operates as two separate antennas, we must now apply this technique to two input impedance loads at the desired operating frequencies within the RFID UHF band, in this case at 927 MHz when the switch is OFF and 902 MHz when the switch is ON. These frequencies are chosen as they are 25 MHz apart; similar, to measured switching-bandwidth shown in Fig. 8. Various techniques for matching complex loads to a real load at two different frequencies have been used; however, they are only applicable for operating frequencies that are largely separated [52]-[56]. Therefore, these techniques are not suitable for our case, where the switching-bandwidth is relatively narrow (e.g., 25 MHz). Consequently, since we cannot design a single matching network that operates simultaneously at both the chosen frequencies, we design the matching network using the average of the two frequencies (i.e., $(927 + 902)/2 \approx 915$ MHz). Since the bandwidth is relatively small (e.g., 25 MHz), this technique works well.

The complex input impedance of our antenna at the desired frequencies of operation are as follows:

$$1.338 + j8.939 \Omega$$
 at 927 MHz (switch OFF) (7)

$$1.079 + j7.444 \Omega$$
 at 902MHz (switch ON) (8)

Notably, these two impedances are approximately equal. Therefore, the problem is simplified in that we only need to match one complex load to 50 Ω . Furthermore, to accommodate the small difference, our matching network (shown in Fig. 11) is designed to provide matching for the average impedance of (7) and (8), i.e., $1.209 + j 8.192 \Omega$, to a 50 Ω load at the average frequency of 915 MHz. The S₁₁ of our antenna with this matching network is shown in Fig. 12.



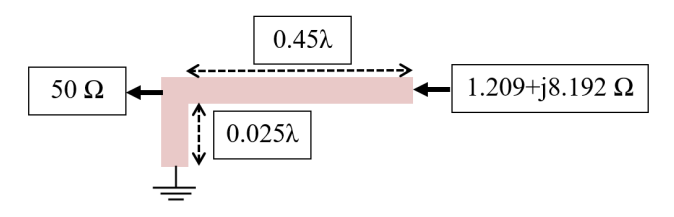


FIGURE 11. First-stage matching network. The input of 1.209 + j8.192 Ω at 902 and 927 MHz is translated to 50 Ω at 906.1 and 923.9 MHz, respectively.

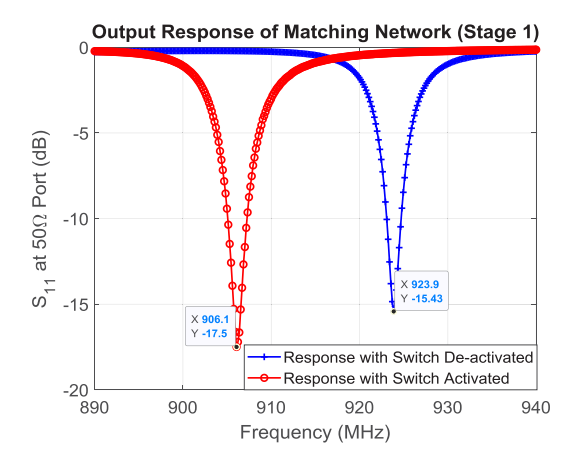


FIGURE 12. Simulated antenna response with the first-stage matching network.

These results confirm that the frequency response of our antenna has been shifted in the RFID UHF band for both states of the switch. It is also observed that the switching bandwidth has decreased from 25 MHz to approximately 18 MHz; however, this bandwidth is still acceptable as it is 70% of the RFID UHF band. This reduction in bandwidth occurs because the matching network cannot support the perfect matching at both 902 and 927 MHz simultaneously, as explained above.

B. SECOND STAGE MATCHING

The purpose of the second stage matching is to match the 50 Ω output response (at the frequencies shown in Fig. 12) of the first stage to the conjugate of the complex load of the RFID IC, i.e., $Z_{IC_CONJ} = 18 + j164 \Omega$. Similar to the design of the first-stage matching, we design the second matching stage at the average frequency of the output response of stage 1 (from Fig. 12) which is 915 MHz. The design of the second stage matching is shown in Fig. 13.

C. FINAL IMPEDANCE MATCHING NETWORK DESIGN AND OPTIMIZATION WITH SIMULATION

The final layout of the two-stage matching network on a substrate with $\varepsilon_r = 12.85$ is depicted in Fig. 14. The transmission line circuit is shortened using meandering [9, pp. 315-319]. Also, the lengths of the transmission lines are optimized using simulation to maximize both the PTC and the switching-bandwidth. Fig. 15 shows the PTC of our

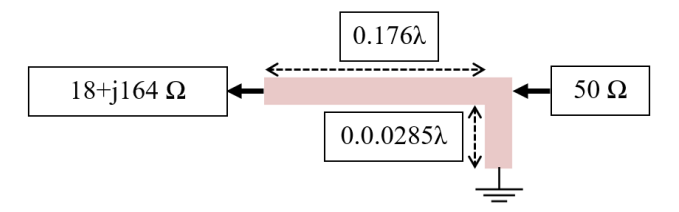


FIGURE 13. Second-stage of matching network. The input of 50 Ω at 906.1 and 923.9 MHz in translated to the conjugate input impedance of the RFID IC at 902.2 and 921.1 MHz, respectively.

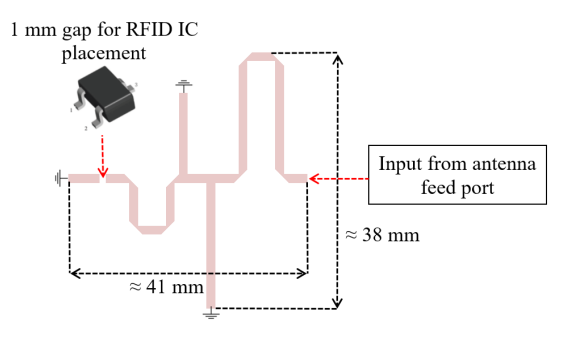


FIGURE 14. Final optimized and miniaturized matching network.

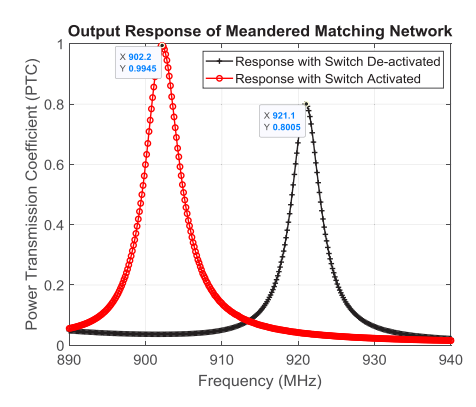


FIGURE 15. Simulated PTC of antenna with final matching network. The final operating frequencies are 921.1 MHz and 902.2 MHz at the OFF (de-activated or de-pressed) and ON states of the switch (activated or pressed), respectively.

antenna with the final matching network which achieves a maximum switching-bandwidth of approximately 19 MHz. It should be noted that the final operating frequencies of our sensor are 921.1 MHz and 902.2 MHz at the OFF and ON states of the switch, respectively.

D. FABRICATION AND MEASUREMENTS

Two versions of the final matching network design shown in Fig. 14 were fabricated and they are depicted in Fig. 16. Version A was fabricated with an IPX miniature (male) port and version B incorporates the RFID IC. Version A was used to test the performance of the matching network using a VNA. Version B was used to test the RFID performance of our sensor.

A coaxial cable with an SMA connector on one end and an IPX connector on the other end is used to connect version A



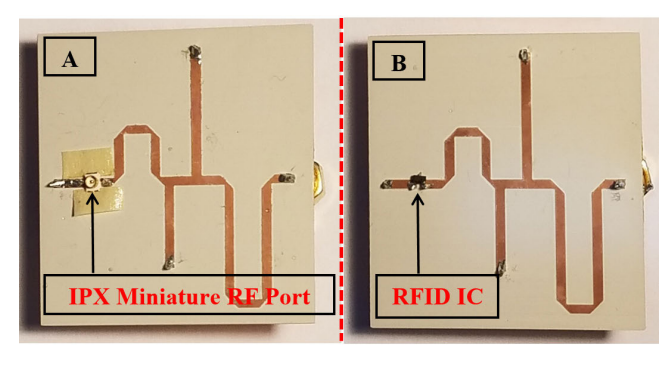


FIGURE 16. Two versions of the matching network are fabricated. (Left) An IPX port is connected for VNA measurement testing. (Right) An RFID IC is connected for RFID testing.

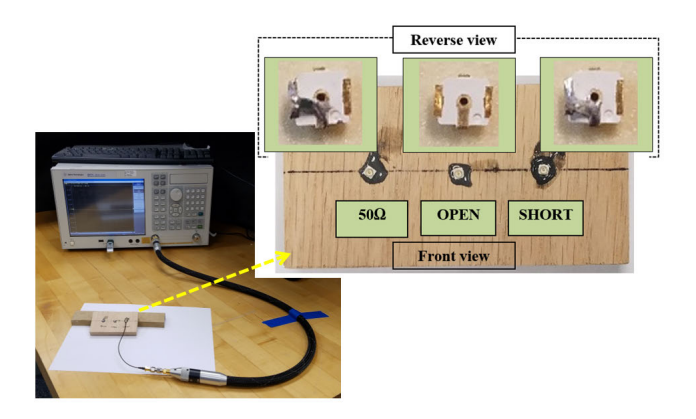


FIGURE 17. VNA setup with custom calibration standards for the IPX to SMA cable extension.

of our prototyped matching network to the VNA. However, this requires calibration, which is accomplished by using our custom IPX open, short and load calibration kit. For the open standard, the port was simply left open. For the short standard, the terminals of the port were soldered (i.e., shorted). Finally, for the load standard, a precision high-frequency surface-mounted 50 Ω resistor was connected between the terminals of the ports [57]. The custom calibration standards along with the VNA calibration setup are shown in Fig. 17.

Once the calibration was performed, the IPX cable was attached to our matching network that was also connected to the antenna, as shown in Fig. 18. After taking the VNA measurements for both states of the switch and using (5), the PTC was calculated and plotted in Fig. 19. As seen, these measured and simulated results agree well. However, there exists a slight shift in the operating frequencies (904 MHz when the switch is OFF and 922.1 MHz when the switch ON) along with a small decrease in the PTC. This is attributed to the male SMA PCB connector used to connect the matching network to the antenna (which could not be accounted for in the calibration process) and due to the tolerance associated with the Rogers TMM13i substrate, which was used to design both the antenna and matching network.

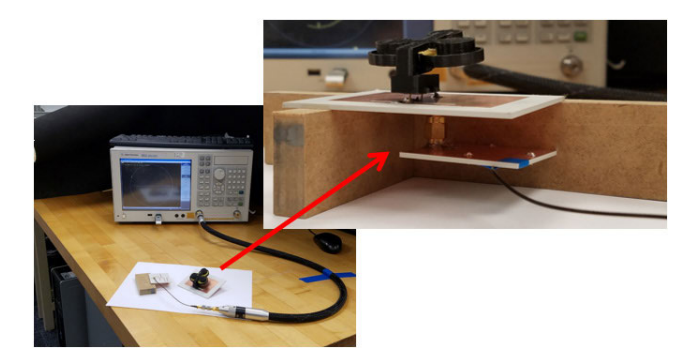


FIGURE 18. The impedance matching network with the IPX port is connected to the antenna. The performance of the design is tested using the VNA.

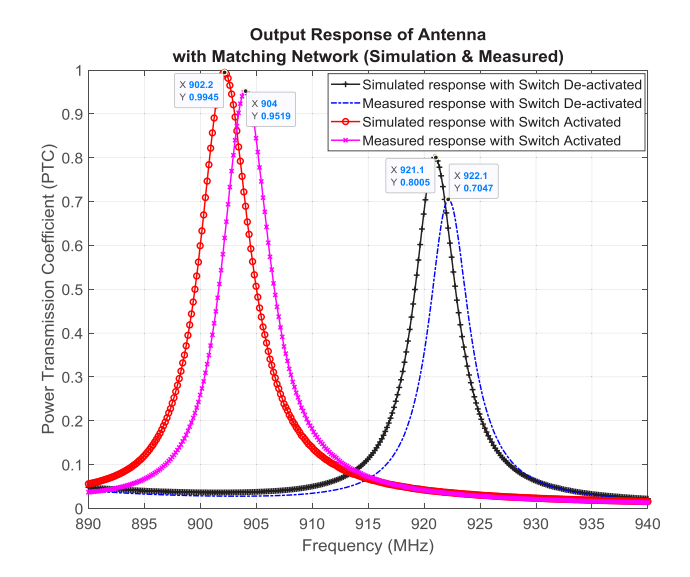


FIGURE 19. Measured and simulated response of the antenna with matching network. When the switch is OFF (not pressed) the measured response is at 922.1 MHz. When the switch is ON (pressed) the measured response is at 904 MHz.

VII. FINAL DESIGN AND RFID PERFORMANCE TESTING

Here, we assemble the complete RFID temperature sensor by combining the designed antenna with the fabricated matching network, which includes the RFID IC that is shown in Fig. 16(b). An enclosure is fabricated to support the antenna structure and the complete sensor is depicted in Fig. 20.

To test the performance of the proposed sensor, we conduct three experiments. In the first one, we use the ThingMagic Pro RFID reader to test the frequency shifting capability of the proposed sensor at the two states of the switch (i.e., in this static test, the switch is actuated manually). In the second one, we validate the temperature-dependent frequency shifting capability using the cold-responsive LCE actuation with a VNA. In the third one, we perform RFID measurements with the proposed sensor in a cold-temperature environment to demonstrate operation in actual working conditions. Finally, in the first and last experiments the test is repeated three times to show consistent operability of the proposed sensor design.

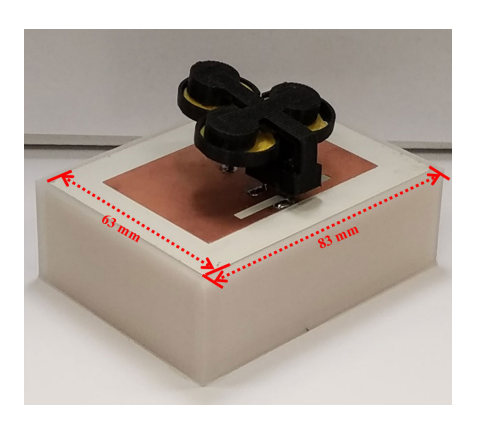


FIGURE 20. Passive RFID temperature sensor.

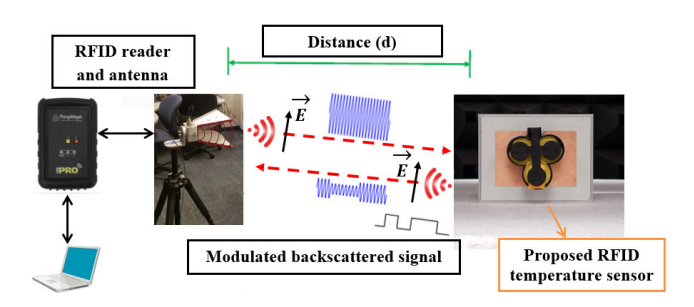


FIGURE 21. Conceptual diagram of the RFID measurement setup.

A conceptual diagram of the RFID measurement setup is depicted in Fig. 21. A linearly polarized double-ridge horn antenna with 7 dBi gain is connected to the RFID reader [58]. Both the reader and the proposed sensor (linearly polarized) are oriented with vertical polarizations. Finally, the RFID measurements are taken as follows. The power of the RFID reader is increased in increments of 0.1 dBm until the threshold power of the RFID IC is reached. The threshold power is identified as the minimum power level at which data begins to be retrieved from the temperature sensor [9, pp. 70-77], [27], [59]. The measured threshold power at which the developed sensor responds is recorded and this procedure is conducted for every frequency in increments of 1 MHz in the 902 to 928 MHz band. The frequency at which the least transmitted power is required to receive data from the tag is therefore the operating frequency.

A. RFID STATIC TESTING

In this section, the switch is actuated manually. The proposed sensor is placed 0.762 m directly in line-of-sight of the reader antenna. The RFID test setup is shown in Fig. 22. The proposed sensor was tested three times for both switch states.

The measured results when the switch is OFF (not pressed or deactivated) are shown in Fig. 23. It is seen that the frequency at which the proposed sensor responds with the minimum transmitted power is at approximately 921 MHz, which agrees with the results of Fig. 19. The measured results when the switch is ON (pressed or activated) are shown in Fig. 24. It is seen that the frequency at which the proposed

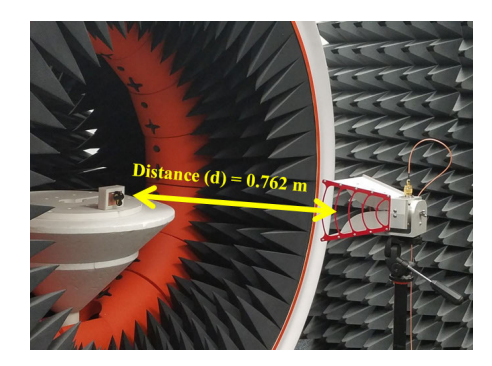


FIGURE 22. Static RFID testing.

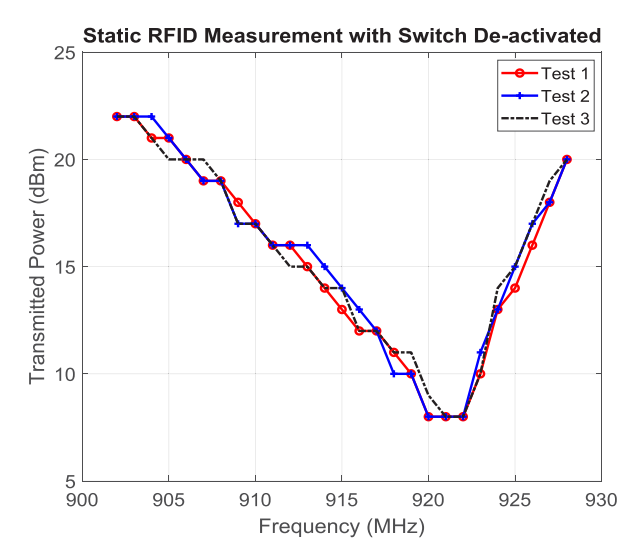


FIGURE 23. Static RFID measurement result with switch OFF.

sensor responds with the minimum transmitted power is at approximately 902 MHz, which again agrees with the results of Fig. 19.

Furthermore, the PTC plots in Fig. 19, show that better matching is achieved when the switch is activated. However, according to Fig. 24, the associated transmitted power required to turn on and read our sensor is higher when the switch is activated. This is expected because the PTC curves in Fig. 19 do not account for the radiation efficiency of the antenna. In fact, according to [60], the radiation efficiency is linearly related to the frequency for a rectangular patch antenna on an electrically thin substrate (with substrate thickness of approximately 1.27 mm and permittivity of 12.85). That is, as frequency increases the radiation efficiency increases. Therefore, more transmitted power is required to turn on and read the sensor for the activated switch-state since it operates at a lower frequency (Fig. 24); even though the matching is better at the activated switch-state (Fig. 19).

B. FREQUENCY SHIFTING USING LCE

In this section, we expose the antenna with the LCE and its support (as shown in Fig. 10) to cold temperatures to demonstrate the switch's actuation by our proposed LCE.



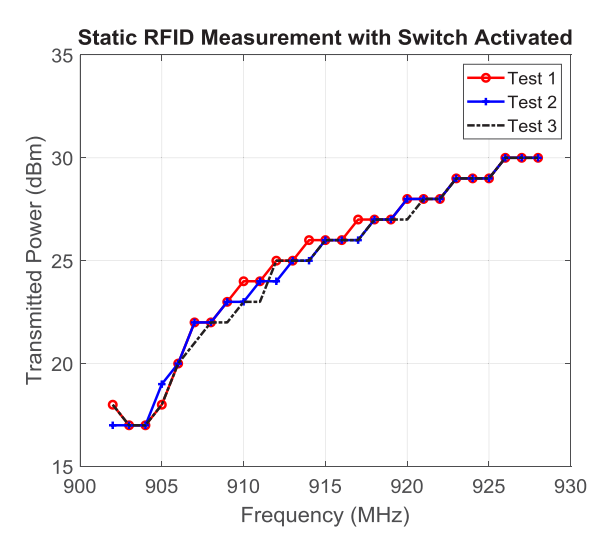


FIGURE 24. Static RFID measurement result with switch ON.

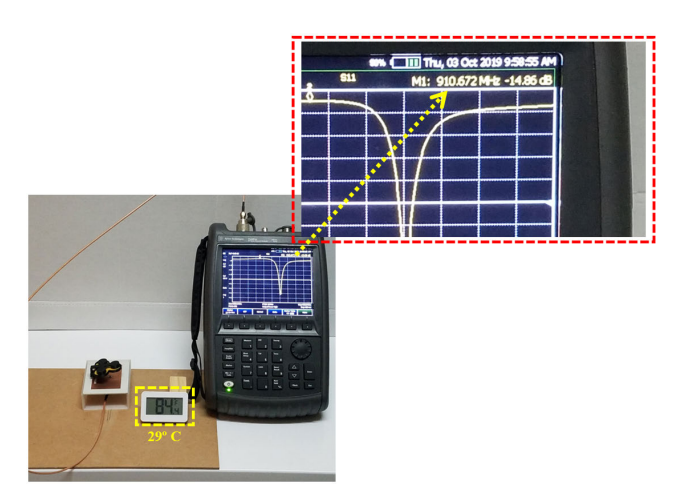


FIGURE 25. The LCE array is relaxed at 29° C. The operating frequency of the antenna design is 910 MHz.

Hence, in this experiment no matching network was used for the antenna and the measurements were taken directly at the output of the antenna. First, the antenna was connected to an Agilent N9923A FieldFox Vector Network analyzer and a measurement was taken at room temperature. This setup is depicted in Fig. 25 where the recorded temperature was 29° C (i.e., 84°F) at the operating frequency of 910 MHz. Subsequently, the antenna was disconnected from the VNA and it was placed inside a freezer along with a digital thermometer. When the temperature threshold of the LCE was reached (e.g., approximately -9° C), the antenna was removed from the freezer and re-connected to the VNA. This setup is shown in Fig. 26, where the recorded temperature was -9° C (i.e., 16°F). Our measurements confirmed that the LCE successfully actuates and triggers the switch, which causes the operating frequency of our tag to shift from 910 MHz to 882 MHz. It is important to note that due to the cold surface of the antenna cooling the surrounding air, condensation is formed on the metallic patch [61]. As a result, in reference to Fig. 8,



FIGURE 26. The LCE array is actuated at -8° C. The switch has been triggered and the operating frequency of the antenna design is 882 MHz.

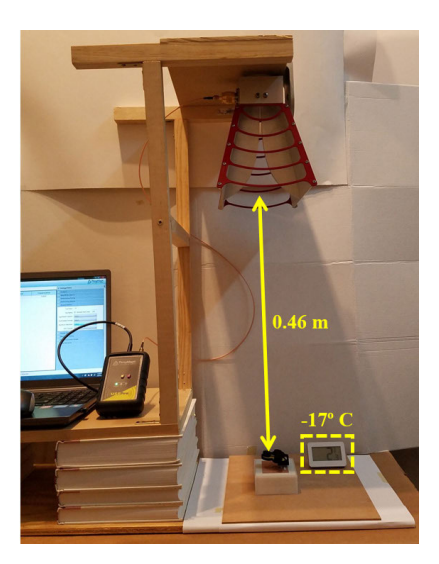


FIGURE 27. Dynamic RFID setup with the designed sensor at -17° C.

this caused a slight shift in the initial operating frequency, which was 885 MHz. Furthermore, as the LCE returns to its relaxed state, the switch automatically deactivates, and the antenna returns to its initial operating frequency, as shown in Fig. 25.

C. RFID DYNAMIC TESTING

In this section, we expose the proposed sensor to cold-temperatures and perform an RFID measurement. The purpose of this measurement is to demonstrate the successful operation (automatic frequency switching ability using an RFID reader) of the sensor in realistic environmental conditions. Similar to the procedure in the previous section, our sensor is placed inside a freezer until the temperature reaches approximately -9° C. Subsequently, the sensor is placed on the test platform, as shown in Fig. 27. In this case, the LCE has been cooled to -17° C and has triggered the switch. The corresponding RFID measurements indicate that the sensor

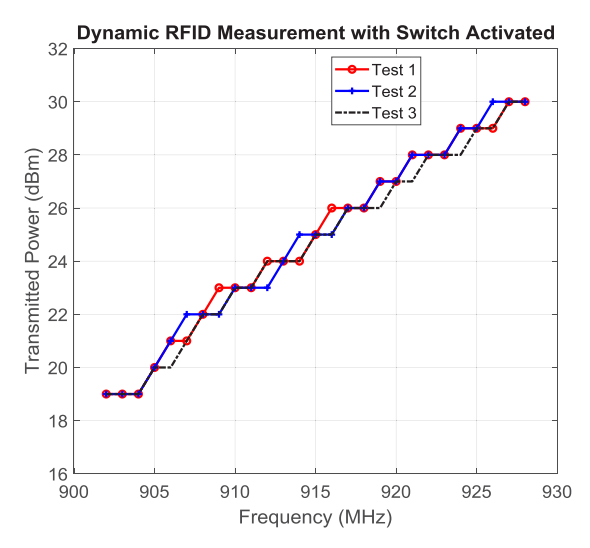


FIGURE 28. Dynamic RFID measurement result with switch ON.

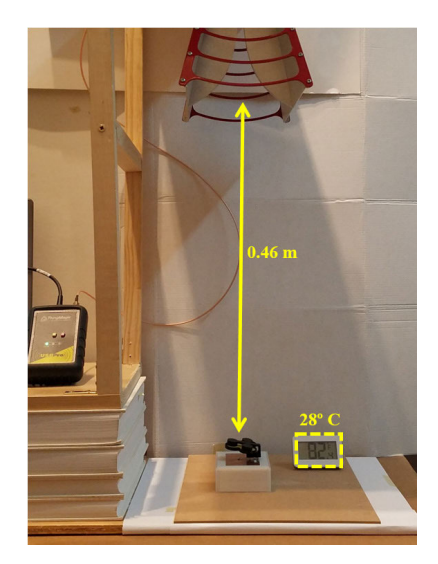


FIGURE 29. Dynamic RFID setup with the designed sensor at 28° C.

responds at 902 MHz as the transmitted power is minimum at this frequency, refer to Fig. 28.

Shortly after, as the temperature raises to the ambient temperature of 28° C, the LCE returns to its relaxed state (without any external intervention), refer to Fig. 29. Consequently, the corresponding RFID measurements indicate that the minimum transmitted power required to receive a response back from the proposed sensor is at approximately 921 MHz (see Fig. 30). These dynamic RFID measurements agree well with the static RFID measurements from Section VII.A. Also, these measurements agree with the VNA measurements shown in Fig. 19. Moreover, these measurements indicate that our design methodology (e.g., the patch antenna with slot that is integrated with a switch and a matching network) works correctly. Notably, the novelty of our passive sensor lies on its autonomous (i.e., no intervention is required), passive (i.e., battery-free) and continuous (i.e., operates through many temperature cycles) operation, which is achieved using

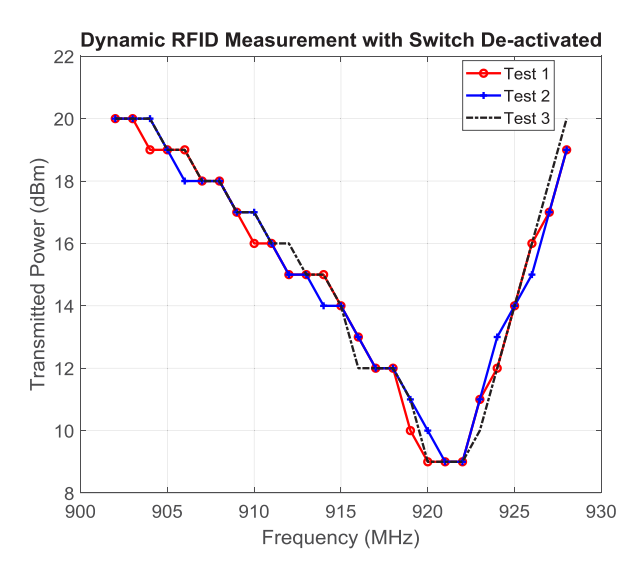


FIGURE 30. Dynamic RFID measurement result with switch OFF.

our novel cold-responsive and reversible LCE technology to actuate the switch.

VIII. CONCLUSION

The current technologies available for monitoring essential foods and medications in the cold supply chain consist of data-loggers, active-devices, or sensors that require resetting. Consequently, these technologies have limitations as they will not provide real-time data, will require repetitive battery changes, will need resetting or will not relay continuous data. Hence, the limitations of such technologies can potentially lead to wasted fresh-food products in the CSC. For these reasons, we developed a new sensor design, which conveys changes in temperature through controlled shifts in the operating frequency within the RFID UHF band. The proposed design is a real-time and purely-passive RFID temperature sensor that can operate autonomously and continuously. Specifically, when a temperature threshold violation occurs, the operating frequency of our sensor shifts. Also, when the temperature is restored, the operating frequency is restored as well without any intervention. Notably, our sensor has the capability to operate through multiple (room-to-cold and cold-to-room) temperature cycles thereby providing critical information about the temperatures that products are exposed to in the cold supply chain. This enables intelligent decision making for accepting of rejecting goods (i.e., foods and medications) based on real-time data, which can minimize waste of goods as well as prevent spoiled goods reaching the market.

The proposed sensor consists of a patch antenna with a slot integrated with a mechanical switch connected across its slot. Moreover, the switch is activated using state-of-the-art 4D printed cold-responsive LCEs. The LCE actuator is designed in a triangular array configuration to provide maximum force.

Also, the theory and operational mechanics of LCEs was presented and the reversible operation of LCEs was demonstrated. Moreover, the design process for our antenna and



its matching network (which provides good matching at two closely spaced frequencies) was discussed. The operation of our RFID sensor was verified through various test setups. Finally, the measured and simulations agreed very well thereby validating our design procedure.

REFERENCES

- Cold Chain Logistics, Cold Supply Chain | Cold Chain Management. Accessed: Dec. 25, 2019. [Online]. Available: https://www.parexel.com/solutions/clinical-research/clinical-trial-supplies-and-logistics/cold-chain-logistics
- [2] Protecting Perishable Foods: During Transport by Truck. Accessed: Dec. 25, 2019. [Online]. Available: https://www.ams.usda.gov/sites/default/files/media/TransportPerishableFoodsbyTruck[1].pdf
- [3] Recommendations on the Control and Monitoring of Storage and Transportation Temperatures of Medicinal Products. Accessed: Dec. 25, 2019. [Online]. Available: https://temptrust.mesalabs.com/wp-content/uploads/sites/47/2012/05/MHRAcon007569.pdf
- [4] (Mar. 23, 2018). Cold Chain—Why is it Growing So Fast? The Logistics of Logistics. Accessed: Oct. 20, 2018. [Online]. Available: https://www. thelogisticsoflogistics.com/cold-chain-growing-fast/
- [5] A. Dada and F. Thiesse. (2018). Sensor Applications in the Supply Chain: The Example of Quality-Based Issuing of Perishables. Accessed: May 14, 2018. [Online]. Available: https://rd.springer.com/ content/pdf/10.1007%2F978-3-540-78731-0_9.pdf
- [6] R. Bhattacharyya, C. Floerkemeier, S. Sarma, and D. Deavours, "RFID tag antenna based temperature sensing in the frequency domain," in *Proc. IEEE Int. Conf. RFID*, Orlando, FL, USA, Apr. 2011, pp. 70–77.
- [7] United World Transportation. (Feb. 22, 2018). The 4 Most Common Cold Chain Logistics Problems Truckers Face and Tips for Solving Them. Accessed: Dec. 25, 2019. [Online]. Available: https://unitedworldtransportation.com/4-common-cold-chain-logistics-problems-truckers-face-tips-solving/
- [8] U. Facts. (2018). Topic: Organic Food Industry. Accessed: May 14, 2018.
 [Online]. Available: https://www.statista.com/topics/1047/organic-food-industry/
- [9] D. Dobkin, The RF in RFID, 1st ed. Amsterdam, The Netherlands: Elsevier, 2008.
- [10] C. Occhiuzzi, S. Caizzone, and G. Marrocco, "Passive UHF RFID antennas for sensing applications: Principles, methods, and classifications," *IEEE Antennas Propag. Mag.*, vol. 55, no. 6, pp. 14–34, Dec. 2013, doi: 10.1109/map.2013.6781700.
- [11] C. Gu, "Fast discrepancy identification for RFID-enabled IoT networks," IEEE Access, vol. 6, pp. 6194–6204, 2018.
- [12] X. Jia, Q. Feng, T. Fan, and Q. Lei, "RFID technology and its applications in Internet of Things (IoT)," in *Proc. 2nd Int. Conf. Consum. Electron.*, *Commun. Netw. (CECNet)*, Yichang, China, Apr. 2012, pp. 1282–1285.
- [13] E. Welbourne, L. Battle, G. Cole, K. Gould, K. Rector, S. Raymer, M. Balazinska, and G. Borriello, "Building the Internet of Things using RFID: The RFID ecosystem experience," *IEEE Internet Comput.*, vol. 13, no. 3, pp. 48–55, May 2009.
- [14] T. Saimounika and K. Kishore, "Real time locating system using RFID for Internet of Things," in *Proc. Int. Conf. Energy, Commun., Data Anal. Soft Comput. (ICECDS)*, 2017, pp. 3507–3508.
- [15] P. Yang, "PRLS-INVES: A general experimental investigation strategy for high accuracy and precision in passive RFID location systems," *IEEE Internet Things J.*, vol. 2, no. 2, pp. 159–167, Apr. 2015.
- [16] W. M. Griggs, R. Verago, J. Naoum-Sawaya, R. H. Ordonez-Hurtado, R. Gilmore, and R. N. Shorten, "Localizing missing entities using parked vehicles: An RFID-based system," *IEEE Internet Things J.*, vol. 5, no. 5, pp. 4018–4030, Oct. 2018.
- [17] N. Choosri, Y. Park, S. Grudpan, P. Chuarjedton, and A. Ongvisesphaiboon, "IoT-RFID testbed for supporting traffic light control," *Int. J. Inf. Electron. Eng.*, vol. 5, no. 2, p. 102, Mar. 2015.
- [18] S. Amendola, R. Lodato, S. Manzari, C. Occhiuzzi, and G. Marrocco, "RFID technology for IoT-based personal healthcare in smart spaces," *IEEE Internet Things J.*, vol. 1, no. 2, pp. 144–152, Apr. 2014.
- [19] W. Jiang, "An intelligent supply chain information collaboration model based on Internet of Things and big data," *IEEE Access*, vol. 7, pp. 58324–58335, 2019.

- [20] A. A. Babar, S. Manzari, L. Sydanheimo, A. Z. Elsherbeni, and L. Ukkonen, "Passive UHF RFID tag for heat sensing applications," *IEEE Trans. Antennas Propag.*, vol. 60, no. 9, pp. 4056–4064, Sep. 2012.
- [21] S. Caizzone, C. Occhiuzzi, and G. Marrocco, "Multi-chip RFID antenna integrating shape-memory alloys for detection of thermal thresholds," *IEEE Trans. Antennas Propag.*, vol. 59, no. 7, pp. 2488–2494, Jul. 2011.
- [22] P. Kumar, H. Reinitz, J. Simunovic, K. Sandeep, and P. Franzon, "Overview of RFID technology and its applications in the food industry," *J. Food Sci.*, vol. 74, no. 8, pp. R101–R106, Oct. 2009.
- [23] Smartrac. Sensor Temperature Dogbone. Accessed: Dec. 25, 2019. [Online]. Available: https://www.smartrac-group.com/sensor-temperature-dogbone.html
- [24] Infratab. Freshtime Tags. Accessed: Dec. 25, 2019. [Online]. Available: https://infratab-dev.myshopify.com/collections/freshtime-tags
- [25] IDS Microship AG. Accessed: Dec. 25, 2019. [Online]. Available: https://www.rfidjournal.net/masterPresentations/live2009/np/Finalist_ IDS_Microship.pdf
- [26] J. S. Gibson, X. Liu, S. V. Georgakopoulos, J. J. Wie, T. H. Ware, and T. J. White, "Reconfigurable antennas based on self-morphing liquid crystalline elastomers," *IEEE Access*, vol. 4, pp. 2340–2348, 2016.
- [27] (2019). Alientechnology. Accessed: Mar. 20, 2018. [Online]. Available: http://www.alientechnology.com/wp-content/uploads/ALC-360-SOT%20Higgs-3%20SOT%20(2016-11-03).pdf
- [28] T. Bjorninen, M. Lauri, L. Ukkonen, R. Ritala, A. Z. Elsherbeni, and L. Sydanheimo, "Wireless measurement of RFID IC impedance," *IEEE Trans. Instrum. Meas.*, vol. 60, no. 9, pp. 3194–3206, Sep. 2011.
- [29] K. RamaDevi, A. M. Prasad, and A. J. Rani, Design of RFID Tag Antennas at UHF Band with Different Materials, 1st ed. Beau-Bassin, Mauritius: LAMBERT Academic, 2018.
- [30] D. Pozar, Microwave Engineering, 4th ed. Hoboken, NJ, USA: Wiley, 2011.
- [31] G. González, Microwave Transistor Amplifiers, 2nd ed. Upper Saddle River, NJ, USA: Prentice-Hall, 1996, p. 47.
- [32] Y. Shafiq, J. S. Gibson, H. Kim, C. P. Ambulo, T. H. Ware, and S. V. Georgakopoulos, "A reusable battery-free RFID temperature sensor," *IEEE Trans. Antennas Propag.*, vol. 67, no. 10, pp. 6612–6626, Oct. 2019.
- [33] P. Nikitin, K. Rao, S. Lam, V. Pillai, R. Martinez, and H. Heinrich, "Power reflection coefficient analysis for complex impedances in RFID tag design," *IEEE Trans. Microw. Theory Techn.*, vol. 53, no. 9, pp. 2721–2725, Sep. 2005.
- [34] M. Bolic, D. Simplot-Ryl, and I. Stojmenović, RFID Systems, 1st ed. Hoboken, NJ, USA: Wiley, 2010.
- [35] F. Yang and Y. Rahmat-Samii, "Patch antennas with switchable slots (PASS) in wireless communications: Concepts, designs, and applications," *IEEE Antennas Propag. Mag.*, vol. 47, no. 2, pp. 13–29, Apr. 2005.
- [36] J. Volakis, (2019). Antenna Engineering Handbook, 5th ed. New York, NY, USA: McGraw-Hill, pp. 829–837.
- [37] (2019). D2F Ultra Subminiature Basic Switch. Accessed: Feb. 7, 2019.
 [Online]. Available: https://media.digikey.com/pdf/Data%20Sheets/ Omron%20PDFs/D2F_0318_DS.pdf
- [38] T. J. White and D. J. Broer, "Programmable and adaptive mechanics with liquid crystal polymer networks and elastomers," *Nature Mater.*, vol. 14, no. 11, pp. 1087–1098, Nov. 2015.
- [39] J. Küpfer and H. Finkelmann, "Nematic liquid single crystal elastomers," *Die Makromolekulare Chem., Rapid Commun.*, vol. 12, no. 12, pp. 717–726, 1991.
- [40] T. H. Ware, M. E. Mcconney, J. J. Wie, V. P. Tondiglia, and T. J. White, "Voxelated liquid crystal elastomers," *Science*, vol. 347, no. 6225, pp. 982–984, Feb. 2015.
- [41] C. P. Ambulo, J. J. Burroughs, J. M. Boothby, H. Kim, M. R. Shankar, and T. H. Ware, "Four-dimensional printing of liquid crystal elastomers," ACS Appl. Mater. Interfaces, vol. 9, no. 42, pp. 37332–37339, Oct. 2017.
- [42] A. Kotikian, R. L. Truby, J. W. Boley, T. J. White, and J. A. Lewis, "3D printing of liquid crystal elastomeric actuators with spatially programed nematic order," *Adv. Mater.*, vol. 30, no. 10, Mar. 2018, Art. no. 1706164.
- [43] M. López-Valdeolivas, D. Liu, D. J. Broer, and C. Sánchez-Somolinos, "4D printed actuators with soft-robotic functions," *Macromol. Rapid Commun.*, vol. 39, no. 5, Mar. 2018, Art. no. 1700710.
- [44] H. Kim, J. Gibson, J. Maeng, M. O. Saed, K. Pimentel, R. T. Rihani, J. J. Pancrazio, S. V. Georgakopoulos, and T. H. Ware, "Responsive, 3D electronics enabled by liquid crystal elastomer substrates," ACS Appl. Mater. Interfaces, vol. 11, no. 21, pp. 19506–19513, May 2019.



- [45] T. Guin, M. J. Settle, B. A. Kowalski, A. D. Auguste, R. V. Beblo, G. W. Reich, and T. J. White, "Layered liquid crystal elastomer actuators," *Nature Commun.*, vol. 9, no. 1, pp. 1–7, 2018.
- [46] C. D. Modes, K. Bhattacharya, and M. Warner, "Disclination-mediated thermo-optical response in nematic glass sheets," *Phys. Rev. E, Stat. Phys. Plasmas Fluids Relat. Interdiscip. Top.*, vol. 81, no. 6, Aug. 2010, Art. no. 060701.
- [47] J. D. Kraus and R. J. Marhefka, Antennas for All Applications, 3rd ed. Boston, MA, USA: McGraw-Hill, 2003, p. 67.
- [48] TMM Thermoset Microwave Materials. Accessed: Dec. 25, 2019. [Online]. Available: https://rogerscorp.com/-/media/project/rogerscorp/documents/advanced-connectivity-solutions/english/data-sheets/tmm-thermoset-laminate-data-sheet-tmm3—-tmm4—-tmm6—-tmm10—-tmm10i—-tmm13i.pdf
- [49] A. Thakur, M. Chauhan, and M. Kumar, "Effect of substrate relative dielectric constant on bandwidth characteristics of line feed rectangular patch antenna," *Int. J. Eng. Sci. Invention Res. Develop.*, vol. 1, pp. 391–396, Apr. 2015.
- [50] R. Garg, P. Bhartia, I. J. Bahl, and A. Ittipiboon, Microstrip Antenna Design Handbook. Boston, MA, USA: Artech House, 2001.
- [51] K. Syuhaimi and M. AbdulMalek, "EM/circuit co-simulation: A highly accurate method for microwave amplifier design," *Univ. J. Comput. Sci. Eng. Technol.*, vol. 2, pp. 127–132, Nov. 2010.
- [52] K. Rawat and F. Ghannouchi, "Dual-band matching technique based on dual-characteristic impedance transformers for dual-band power amplifiers design," *IET Microw. Antennas Propag.*, vol. 5, no. 14, p. 1720, 2011.
- [53] X. Zheng, Y. Liu, S. Li, C. Yu, Z. Wang, and J. Li, "A dual-band impedance transformer using pi-section structure for frequency-dependent complex loadS," *Prog. Electromagn. Res. C*, vol. 32, pp. 11–26, 2012, doi: 10.2528/pierc12052909.
- [54] M.-L. Chuang, "Dual-band impedance transformer using two-section shunt stubs," *IEEE Trans. Microw. Theory Techn.*, vol. 58, no. 5, pp. 1257–1263, Apr. 2010, doi: 10.1109/tmtt.2010.2045560.
- [55] M. A. Maktoomi, V. Panwar, M. S. Hashmi, and F. M. Ghannouchi, "A dual-band matching network for frequency-dependent complex loads suitable for dual-band RF amplifiers," in *Proc. IEEE Int. Microw. RF Conf. (IMaRC)*, Bangalore, India, Dec. 2014, pp. 88–91, doi: 10.1109/ IMaRC.2014.7038977.
- [56] M. Nikravan and Z. Atlasbaf, "T-section dual-band impedance transformer for frequency-dependent complex impedance loads," *Electron. Lett.*, vol. 47, no. 9, pp. 551–553, Apr. 2011, doi: 10.1049/el.2010.7452.
- [57] High Frequency (Up to 40 GHz) Resistor, Thin Film Surface Mount Chip. Accessed: Dec. 25, 2019. [Online]. Available: http://www.vishay.com/. http://www.vishay.com/docs/60093/fcseries.pdf
- [58] Model: SAS-571. Accessed: Dec. 25, 2019. [Online]. Available: https://www.atecorp.com/atecorp/media/pdfs/data-sheets/ah-systems-sas-571_datasheet.pdf
- [59] X. Yi, T. Wu, Y. Wang, and M. M. Tentzeris, "Sensitivity modeling of an RFID-based strain-sensing antenna with dielectric constant change," *IEEE Sensors J.*, vol. 15, no. 11, pp. 6147–6155, Nov. 2015.
- [60] S. K. Behera, "Novel tuned rectangular patch antenna as a load for phase power combining," Ph.D. dissertation, Dept. Electron. Telecommun. Eng., Jadavpur Univ., Kolkata, India, 2002, p. 18.
- [61] Preventing Condensation. Accessed: Dec. 25, 2019. [Online]. Available: https://www.vaisala.com/sites/default/files/documents/ PreventingCondensation.pdf



YOUSUF SHAFIQ (Student Member, IEEE) received the B.S. and M.S. degrees in electrical engineering from Florida International University (FIU), Miami, FL, USA, in 2009 and 2010, respectively, where he is currently pursuing the Ph.D. degree in electrical engineering.

From 2010 to 2012, he worked as a Communications Systems Engineer with Lockheed Martin Space Systems, Newtown, PA, USA. Subsequently, he worked as an RCS Engineer at

Pratt and Whitney, West Palm Beach, FL, USA. Finally, from 2014 to 2017, he was an Electrical Engineer with the Naval Surface Warfare Center, Panama City Beach, FL, USA. He is also a Research Assistant with the RFCOM Lab, FIU. His current research interest is in wireless sensing using innovative reactive materials combined with novel antenna and RF circuit design techniques.



JULIA HENRICKS received the B.S. degree in biomedical engineering from The University of Texas at Dallas, in 2018, and the Ph.D. degree in biomedical engineering, in 2019. She is currently works as a Reliability Engineer at Abbott Laboratories, testing Alinity s Blood and Plasma Screening devices. She worked on light-responsive materials and temperature-responsive materials for antennas and implantable devices.



CEDRIC P. AMBULO received the B.A. degree in physics from Austin College, in 2016. He joined the Ware Research Lab, The University of Texas at Dallas, in the Fall of 2016. He is currently researching and developing stimuli-responsive, liquid crystal elastomer actuators toward soft robotic applications.



TAYLOR H. WARE received the B.S. degree from the Georgia Institute of Technology, in 2009, and the M.S. and Ph.D. degrees from The University of Texas at Dallas, in 2011 and 2013, respectively. From 2013 to 2015, he was a Post-doctoral Researcher at the Air Force Research Laboratory. Since 2015, he has been an Assistant Professor with the Bioengineering Department, The University of Texas at Dallas. His research interests include liquid crystal materials, flexible

electronics, and biomaterials.



STAVROS V. GEORGAKOPOULOS (Senior Member, IEEE) received the Diploma degree in electrical engineering from the University of Patras, Patras, Greece, in June 1996, and the M.S. degree in electrical engineering and the Ph.D. degree in electrical engineering from Arizona State University (ASU), Tempe, AZ, USA, in 1998 and 2001, respectively.

From 2001 to 2007, he held a position as the Principal Engineer at SV Microwave, Inc. Since

2007, he has been with the Department of Electrical and Computer Engineering, Florida International University, Miami, FL, USA, where he is currently a Professor, the Director of the Transforming Antennas Center (a research center on foldable/origami, physically reconfigurable and deployable antennas), and the Director of the RF Communications, Millimeter-Waves, and Terahertz Lab. His current research interests relate to novel antennas, arrays, RFID, microwave and RF systems, novel sensors and wireless powering of portable, as well as wearable and implantable devices.

Dr. Georgakopoulos received the 2015 FIU President's Council Worlds Ahead Faculty Award, which is the highest honor FIU extends to a faculty member for excelling in research, teaching, mentorship, and service. He serves as an Associate Editor of the IEEE Transactions on antennas and propagation (2013–2019) and as an Associate Editor of the IEEE Open Journal of Antennas and Propagation (2019–present).